The diagnostic capabilities of polarization-correlation analysis of scattered light in biological tissues to differentiate between benign and malignant tumors

Iryna Soltys[a], Alexander Olar[a], Natalia Pavlyukovich[b], Yelena Kurek[a], Alexander Salega[a], Yaroslav Struk[a], Oleg Vanchulyak[b], Igor Oliynyk[b], Iryna Drin[a]

[a]Yuriy Fedkovich Chernivtsi National University, Chernivtsi, Ukraine, 58012
[b]Bukovinian State Medical University, Chernivtsi, Ukraine, 58009

ABSTRACT

The provided materials present the results of the diagnostic application of polarization-correlation cartography of microscopic images of the polycrystalline component of biological tissues for the differential diagnosis of benign (adenoma) and malignant (adenocarcinoma) prostate tumors. For microscopic images of histological sections of adenoma and adenocarcinoma biopsies, integral and layered maps, as well as histograms of the distributions of the following parameters are provided:
1. The modulus of the fourth parameter $|SK_4^{12}|$ of the polarization-correlation vector.
2. The argument of the fourth parameter $Arg(S_4^{12})$ of the polarization-correlation vector.
Systematized tables contain the values of central statistical moments of the 1st to 4th order, which characterize the polarization-correlation, wavelet, and multifractal parameters of the polarization-correlation maps $|SK_4^{12}|(m \times n)$ and $Arg(S_4^{12})(m \times n)$. Additionally, a set of the most sensitive diagnostic markers has been determined, representing statistical parameters that are highly responsive to changes in the polycrystalline structure of biological samples.
Keywords: polarization, correlation analysis, tumor, scattered light.

1. INTRODUCTION

The vast majority of scientific research in the field of biomedical polarimetry is focused on utilizing various methods of statistical, correlation, fractal singular, and other analyses of distributions from experimental data, such as polarization and Mueller matrix maps of biological samples[1-9]. All these methods share a common platform, known as the "single-point" approach, where the analysis of experimental information occurs from point to point in the coordinate distribution. However, this approach leads to the loss of information about the topographical structure of polarization and Mueller matrix maps of biological samples.

Our work is aimed at testing a different "dual-point" approach, or polarization corneometry of polarization and Mueller matrix maps of prostate tumor biological samples. In this approach, we aim to retain the topographical information of the structural features present in the polarization and Mueller matrix maps[10-14], allowing for a more comprehensive analysis and potentially enhancing the diagnostic capabilities for prostate tumor samples.

2. POLARIZATION-CORRELATION MAPS OF MICROSCOPIC IMAGES OF HISTOLOGICAL SECTIONS OF PROSTATE ADENOMA AND ADENOCARCINOMA

To implement the complex diagnostic polarization-correlation research[10-12], two groups of histological section samples of prostate tumors were formed:
- Adenoma - Control Group 1, consisting of 19 samples.
- Adenocarcinoma - Experimental Group 2, consisting of 19 samples.

The optico-geometric parameters of the samples are provided in the following table

Parameters	
Geometric thickness, h, µm	40 – 45
Optical thickness, τ µm	0,25 – 0,28
Degree of depolarization, Δ, %	29 – 33

Figure 1 shows:

1. Layered $\mu = \pi/8$ maps $|SK_4^{12}|(m \times n)$ (fragments (1), (2)) of histological sections of biopsy samples from group 1 (fragments (1)) and group 2 (fragments (2)) tumors.
2. Histograms of the distribution of $|SK_4^{12}|(m \times n)$ microscopic images of histological sections of adenoma from group 1 (fragments (3)) and group 2 (fragments (4)).

The results of the statistical and informational analysis of the polarization-correlation maps $|SK_4^{12}|(m \times n)$ of microscopic images of histological sections of adenoma and carcinoma biopsy samples are presented in Table 1. The comparative analysis of the obtained data on the layered structure of polarization-correlation maps of the module $|SK_4^{12}|(m \times n)$ of microscopic images of histological sections of benign and malignant prostate tumors from both groups revealed the following:

1. For malignant conditions, there is a minimal (within 10%-15%) decrease in the magnitude of the first and second-order statistical moments $Z_{i=1;2}(|SK_4^{12}|(m \times n))$, as shown in Table 1.
2. On the contrary, the statistical moments of higher orders, which characterize the asymmetry and excess of the distributions of $|SK_4^{12}|(m \times n)$ samples from group 2, slightly increase, as shown in Table 1.
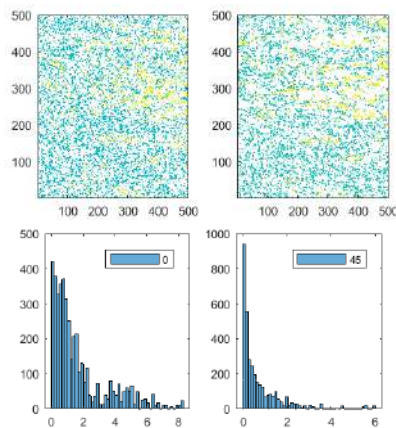

Figure 1. Polarization-correlation maps $|SK_4^{12}|(m \times n)$ (top row) and histograms $G(|SK_4^{12}|)$ of $|SK_4^{12}|$ | distributions (bottom row) in the phase plane μ=π/8 of microscopic images of histological sections of biopsy samples from adenoma (left column) and carcinoma (right column)

Table 1. Statistical moments $Z_{i=1,2,3,4}$, characterizing the distributions of the polarization-correlation parameter $|SK_4^{12}|(m \times n)$ of microscopic images of histological sections of biopsy samples from adenoma and carcinoma of the prostate - phase plane $\mu = \pi/8$

$Z_{i=1,2,3,4}$	Group 1	Group 2	$Ac, \%$
Z_1	0,087±0,005	0,074±0,005	82,4
Z_2	0,103±0,006	0,088±0,006	82,4
Z_3	1,93±0,11	2,28±0,12	85,3
Z_4	3,19±0,17	3,68±0,19	85,3

The obtained results show that the balanced accuracy of differential diagnosis between adenoma and adenocarcinoma samples is low - unsatisfactory, $Ac < 80\%$ (Table 1) or satisfactory, $Ac \sim 82\% - 85\%$.

From a physical standpoint, this result can be explained by the fact that the magnitude of $|SK_4^{12}|(m \times n)$ is determined by the level of circular birefringence of optically active molecular domains. For different stages of oncological changes, their concentration does not undergo significant changes. Therefore, the differences between the polarization-correlation maps $|SK_4^{12}|(m \times n)$ of microscopic images of histological sections of adenoma and adenocarcinoma of the prostate are minimal, resulting in low accuracy in differentiating between these conditions.

3. POLARIZATION-CORRELATION MAPS OF $Arg(S_4^{12})(m \times n)$ FOR MICROSCOPIC IMAGES OF HISTOLOGICAL SECTIONS OF PROSTATE ADENOMA AND ADENOCARCINOMA

Figure 2 shows:

- Layered $\mu = \pi/8$ (Figure 2) maps of the argument $Arg(S_4^{12})(m \times n)$ (fragments (1),(2)) of histological sections of tumors from group 1 (fragments (1)) and group 2 (fragments (2)).
- Histograms of the distribution of $Arg(S_4^{12})(m \times n)$ microscopic images of histological sections of adenoma from group 1 (fragments (3)) and group 2 (fragments (4)).

Comparative analysis of the obtained data on the layered structure of polarization-correlation maps of the argument $Arg(S_4^{12})(m \times n)$ from microscopic images of histological sections of benign and malignant prostate tumors from both groups revealed:

- For the malignant condition, there is a minimal (within 12%-17%) decrease in the values of the first and second-order statistical moments $Z_{i=1;2}(Arg(S_4^{12})(m \times n))$, - Table 2.
- The higher-order statistical moments, characterizing the asymmetry and excess of the distributions of $Arg(S_4^{12})(m \times n)$ from samples in group 2, on the contrary, significantly increase, - Table 2. As a result, the balanced accuracy of the differential diagnosis of adenoma and adenocarcinoma samples increases to a satisfactory level $Ac \sim 82,4\%$ for the phase cross-section $\mu = {}^{\pi}/_8$.
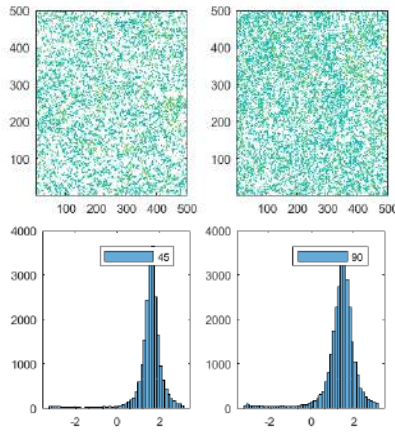

Figure 2. Polarization-correlation maps $Arg(S_4^{12})(m \times n)$ ((top row) and histograms $G(Arg(S_4^{12}))$) (bottom row) of the distributions of $Arg(S_4^{12})$ in the phase plane μ=π⁄8 of microscopic images of histological sections of adenoma (left column) and adenocarcinoma (right column).

The results of the statistical and informational analysis of the polarization-correlation maps $Arg(S_4^{12})(m \times n)$ of microscopic images of histological sections of adenoma and adenocarcinoma are presented in Table 2.

Table 2 Statistical moments $Z_{i=1,2,3,4}$ characterizing the distributions of the polarization-correlation parameter $Arg(S_4^{12})(m \times n)$ of microscopic images of histological sections of adenoma and adenocarcinoma of the prostate - phase plane $\mu = \pi/8$

$Z_{i=1,2,3,4}$	Group 1	Group 2	$Ac, \%$
Z_1	0,098±0,005	0,087±0,005	82,4
Z_2	0,113±0,006	0,099±0,006	82,4
Z_3	1,62±0,09	1,98±0,11	88,2
Z_4	2,32±0,13	2,97±0,16	88,2

4. CONCLUSIONS

From a physical perspective, the observed results can be explained by the fact that the parameter $Arg(S_4^{12})$ of polarization-correlation manifestations in an optically thin biological layer with complex linear LB and circular CB birefringence

predominantly depends on the parameters of structural anisotropy (distributions of optical axis directions ρ and phase shift values δ between linearly and orthogonally polarized components of the laser radiation amplitude) - $Arg(SK_4^{12}) \sim (\delta_1 sin\rho_1 + \delta_2 sin\rho_2)^{-1}$. For different stages of oncological changes, this structure undergoes significant alterations. In malignant conditions, due to necrotic states, the fibrils become disordered and refined. As a result, the differences between polarization-correlation maps of $Arg(S_4^{12})(m \times n)$ of microscopic images of histological sections of adenoma and adenocarcinoma of the prostate increase, and the accuracy of the differential diagnosis for such conditions reaches a good level.

REFERENCES

[1] Peyvasteh, M., Dubolazov, A. Popov, A. et.al. "Two-point Stokes vector diagnostic approach for characterization of optically anisotropic biological tissues," Journal of Physics D: Applied Physics 53 (39), 395401 (2021).

[2] Angelsky, O., Bekshaev, A., Dragan, G., Maksimyak, P., Zenkova, C., Zheng, J. (2021) Structured Light Control and Diagnostics Using Optical Crystals," Front. Phys. 9:715045 (2021).

[3] Angelsky, O., Maksimyak, P. "Polarization-interference measurement of phase-inhomogeneous objects," Appl. Opt. 31, 4417-4419 (1992).

[4] Angelsky, O., Maksymyak, P., Zenkova, C., etc. "Peculiarities of control of erythrocytes moving in an evanescent field," Journal of Biomedical Optics 24(5), 055002 (2019).

[5] Angelsky, O.V., Zenkova, C.Y., Maksymyak, P.P. et al. "Peculiarities of Energy Circulation in Evanescent Field. Application for Red Blood Cells," Opt. Mem. Neural Networks 28, 11–20 (2019).

[6] ANGELSKY, O. V. et al. "Experimental demonstration of singular-optical colouring of regularly scattered white light," Journal of the European Optical Society 3, (2008).

[7] Ushenko, V., Dubolazov, A., Pidkamin, L., et.al. "Mapping of polycrystalline films of biological fluids utilizing the Jones-matrix formalism," Laser Physics 28 (2), 025602 (2021).

[8] Tereikovskyi, I., Zhengbing Hu, Denys Chernyshev, Liudmyla Tereikovska, Oleksandr Korystin, Oleh Tereikovskyi, "The Method of Semantic Image Segmentation Using Neural Networks,", International Journal of Image, Graphics and Signal Processing (IJIGSP), 14(6), 1-14 (2022).

[9] Kamal Omprakash Hajari, Ujwalla Haridas Gawande, Yogesh Golhar, "Motion Pattern Based Anomalous Pedestrian Activity Detection," International Journal of Image, Graphics and Signal Processing(IJIGSP), 14(6), 15-25 (2022).

[10] Zaliskyi, M. etc. "Shadow Image Processing of X-Ray Screening System for Aviation Security," International Journal of Image, Graphics and Signal Processing(IJIGSP), 14(6), 26-46 (2022).

[11] Sithmini Gunasekara, Dilshan Gunarathna, Maheshi B. Dissanayake, Supavadee Aramith, Wazir Muhammad "Deep Learning Based Autonomous Real-Time Traffic Sign Recognition System for Advanced Driver Assistance," International Journal of Image, Graphics and Signal Processing(IJIGSP) 14(6), 70-83 (2022).

[12] Jiashu, Xu, Stirenko, S. " Self-Supervised Model Based on Masked Autoencoders Advance CT Scans Classification," International Journal of Image, Graphics and Signal Processing(IJIGSP) 14(5), 1-9 (2022).

[13] Tereikovskyi, I. etc. "The Method of Semantic Image Segmentation Using Neural Networks," International Journal of Image, Graphics and Signal Processing(IJIGSP) 14(6), 1-14 (2022).

[14] Kamal Omprakash Hajari, Ujwalla Haridas Gawande, Yogesh Golhar, "Motion Pattern Based Anomalous Pedestrian Activity Detection," International Journal of Image, Graphics and Signal Processing(IJIGSP) 14(6), 15-25 (2022).

ACKNOWLEDGMENT